

A Convergence Study of the 3D Dynamic Diffusion Method

Ramoni Z. S. Azevedo[1(✉)], Lucia Catabriga[1,2(✉)], and Isaac P. Santos[1,3(✉)]

[1] Laboratório de Otimização e Modelagem Computacional, Programa de Pós-Graduação em Informática, Universidade Federal do Espírito Santo, Vitória, ES, Brazil
ramoni.sedano@aluno.ufes.br

[2] Departamento de Informática, Universidade Federal do Espírito Santo, Vitória, ES, Brazil
luciac@inf.ufes.br

[3] Departamento de Matemática Aplicada, Universidade Federal do Espírito Santo, São Mateus, ES, Brazil
isaac.santos@ufes.br

Abstract. In this work we present a convergence study of the multi-scale Dynamic Diffusion (DD) method applied to the three-dimensional steady-state transport equation. We consider diffusion-convection and diffusion-convection-reaction problems, varying the diffusion coefficient in order to obtain an increasingly less diffusive problem. For both cases, the convergence order estimates are evaluated in the energy norm and the $L^2(\Omega)$ and $H^1(\Omega)$ Sobolev spaces norms. In order to investigate the meshes effects on the convergence, the numerical experiments were carried out on two different sets of meshes: one with structured meshes and the other with unstructured ones. The numerical results show optimal convergence rates in all norms for the dominant convection case.

Keywords: Dynamic diffusion method · Convergence estimate · 3D transport equation

1 Introduction

Let $\Omega \subset \mathbb{R}^3$ be a bounded domain with a Lipschitz boundary Γ with an outward unit normal $\boldsymbol{n}$. The steady-state diffusive–convective–reactive transport problem is described by

$$-\kappa \Delta u + \boldsymbol{\beta} \cdot \boldsymbol{\nabla} u + \sigma u = f \quad \text{in } \Omega, \tag{1}$$

$$u = u_D \quad \text{on } \Gamma, \tag{2}$$

where u represents the quantity being transported, $\kappa > 0$ is the diffusivity coefficient, $\boldsymbol{\beta} \in [L^\infty(\Omega)]^3$ is the velocity field such that $\boldsymbol{\nabla} \cdot \boldsymbol{\beta} = 0$, $\sigma \geq 0$ is the reaction coefficient, $f \in L^2(\Omega)$ is the source term and $u_D \in H^{1/2}(\Gamma)$.

© Springer Nature Switzerland AG 2021
O. Gervasi et al. (Eds.): ICCSA 2021, LNCS 12949, pp. 62–77, 2021.
https://doi.org/10.1007/978-3-030-86653-2_5

This equation plays an important role in many study fields such as dispersal of pollutants [1], chemical reaction [2], deterministic and continuous population models in ecology and economy [3], flow of large crowds of pedestrians [4], trickle-bed reactors that are employed in hydrotreatments and hydrocracking reactions in the petrochemical processing industries to the environmental detoxification of exhaust gases and polluted wastewaters from chemical plants [5], petroleum wellbore stability [6]. Due to the difficulty of solving analytically the mathematical models related to those applications, several numerical methods, such as finite differences, finite elements, finite volumes and boundary elements, have been developed to obtain approximate solutions of problem (1)–(2) [7].

In the context of finite element methods, the usual approach to cope with the instabilities caused by the convection (or reactive) term is to add extra operators to the standard Galerkin formulation with the aim of increasing the stability of the approximate solution. In general, these new formulations involves the Galerkin method coupled with two operators, one defining linear stabilized formulations and the other nonlinear, the so-called shock-capturing term. Some well-known linear stabilized formulations are the Streamline Upwind Petrov-Galerkin (SUPG) method [8], the Galerkin-Least Square (GLS) method [9], the Unusual Finite Element Method (USFEM) [10], the Continuous Interior Penalty (CIP) method [11] and the Local Projection Stabilization (LPS) [12]. Although all these linear methods present stable global solutions, non-negligible spurious oscillations are often present in the neighborhood of sharp layers. In order to recover the monotonicity properties of the continuous problem, precluding under/overshoots in the boundary layers, one can resort to the nonlinear stabilized methods. See [13,14] for an excellent review about classical nonlinear shock-capturing schemes.

The linear stabilized methods, such as SUPG, GLS, CIP and LPS, using linear interpolation, present convergence estimates with theoretical order of $\mathcal{O}(h^{3/2})$ and $\mathcal{O}(h)$ in the norms of the Sobolev spaces, $L^2(\Omega)$ and $H^1(\Omega)$, respectively, where h is the mesh size parameter [9,11,12,15]. The estimate in $H^1(\Omega)$ is optimal, whereas in $L^2(\Omega)$ is sub-optimal, leaving a gap of $\mathcal{O}(h^{1/2})$ in the order of convergence in the L^2-norm. According to [16], in general, shock-capturing schemes exhibit a priori error estimates of $\mathcal{O}(h^{1/2})$ for linear interpolants and using a mesh dependent norm, although some nonlinear methods are designed to present better convergence estimates, such as the methods presented in [17,18].

Another class of methods for solving convection dominated problems is based on the variational multiscale (VMS) framework, introduced by Hughes et al. in [19,20]. In particular, we mention the nonlinear two-scales formulations developed in [21–26]. These two-scales methods consists of adding locally and dynamically a nonlinear artificial diffusion either on the subgrid scale [24,25] or on both scales [21,26], in order to achieve stability of the numerical solution. This methodology has been applied for solving 2D problems, such as scalar transport equations, compressible and incompressible flow problems, obtaining good results [22,23,26]. In [27] the nonlinear two-scale method proposed in [21,26],

called the Dynamic Diffusion (DD) method, was applied for solving 3D scalar transport equations with convection dominant.

The numerical analysis of the DD method shares the difficulties of classical nonlinear shock-capturing methods. In [28] is presented a numerical analysis of a variant of the DD method, obtaining a theoretical convergence estimate of order $\mathcal{O}(h^{1/2})$ in the energy norm, although the numerical experiments show optimal convergence in the $L^2(\Omega)$ and $H^1(\Omega)$ norms. In [26], a numerical study of the convergence estimates of the DD method, in the solution of two-dimensional problems, was carried out, obtaining optimal convergence rates on the $L^2(\Omega)$ and $H^1(\Omega)$ norms. This study is extended here for three-dimensional problems.

The aim of this work it to present a convergence study of the DD method when it is applied for solving 3D problems. We evaluated the convergence order estimates in the energy norm and the norms of the Sobolev spaces, $L^2(\Omega)$ and $H^1(\Omega)$, considering two transport equations for both, convection and diffusion dominant regimes. The numerical experiments was carried out on two different sets of meshes in order to investigate the mesh effects on the convergence order.

The remainder of this work is organized as follows. In Sect. 2 we present the numerical formulation of the DD method. In Sect. 3 the numerical experiments are conducted and the conclusions of the this paper are described in Sect. 4.

2 Dynamic Diffusion Method

The DD method is a nonlinear multiscale method that consists of adding a nonlinear artificial diffusion operator acting on both scales of the discretization [21,26]. The multiscale method is proposed by defining the enriched spaces S_E and V_E, spaces of admissible functions and test functions, as $S_E = S_h \oplus S_B$ and $V_E = V_h \oplus S_B$, where

$$S_h = \{u_h \in H^1(\Omega) : u_h|_{\Omega_e} \in \mathbb{P}_1(\Omega_e), \forall \Omega_e \in \mathcal{T}_h, u_h = g \in \Gamma\},$$
$$V_h = \{v_h \in H^1(\Omega) : v_h|_{\Omega_e} \in \mathbb{P}_1(\Omega_e), \forall \Omega_e \in \mathcal{T}_h, v_h = 0 \in \Gamma\}$$

are the discrete spaces of the Galekin method for linear tetrahedral elements (see [27] for more details), and S_B is the space spanned by bubble functions. By denoting $N_b \in H_0^1(\Omega^e)$ as the bubble function defined in each element Ω_e, we define $S_B|_{\Omega_e} = span(N_b)$ and $S_B = \oplus|_{\Omega_e} S_B|_{\Omega_e}$ for all Ω_e in $\mathcal{T}_h$. Here, we use $N_b = 256 N_1(x,y,z)N_2(x,y,z)N_3(x,y,z)N_4(x,y,z)$, where N_j is the local interpolation function associated with the nodal point j of the element Ω_e [29].

The DD method can be statement as: find $u = u_h + u_b \in S_E$, with $u_h \in S_h$ and $u_b \in S_B$, such that,

$$A(u,v) + A_{DD}(u_h; u, v) = F(v), \tag{3}$$

for all $v = v_h + v_b \in V_E$, with $v_h \in V_h$ and $v_b \in S_B$, where

$$A(u,v) = \int_{\Omega_e} \kappa \boldsymbol{\nabla} u \cdot \boldsymbol{\nabla} v + (\boldsymbol{\beta} \cdot \boldsymbol{\nabla} u) v + \sigma u v \, d\Omega_e,$$

$$A_{DD}(u_h; u, v) = \int_{\Omega_e} \tau_{DD}(u_h) \boldsymbol{\nabla} u \cdot \boldsymbol{\nabla} v \; d\Omega_e,$$
$$F(v) = \int_{\Omega_e} f v \; d\Omega_e.$$

In the nonlinear operator $A_{DD}(u_h; \cdot, \cdot)$, the function $\tau_{DD}(u_h)$ represents the amount of artificial diffusion and is defined as

$$\tau_{DD}(u_h) = \begin{cases} \mu(h) \frac{|R(u_h)|}{\|\boldsymbol{\nabla} u_h\|}, & \text{if } \|\boldsymbol{\nabla} u_h\| > 0, \\ 0, & \text{otherwise,} \end{cases} \tag{4}$$

where

$$R(u_h) = -\kappa \Delta u_h + \boldsymbol{\beta} \cdot \boldsymbol{\nabla} u_h + \sigma u_h - f \tag{5}$$

is the residue of the resolved scale of the equation, calculated in the barycenter of the element Ω_e. The symbol $|\cdot|$ represents the module of a real number and $\|\cdot\|$ is the Euclidean norm. The parameter $\mu(h)$ is given by

$$\mu(h) = \begin{cases} \frac{3}{4} \left(\sqrt[3]{V_e} + \frac{\|\boldsymbol{\beta}_B\|}{\|\boldsymbol{B}\|} \right), & \text{if } \Omega_e \cap \Gamma_+ \neq \emptyset, \\ \frac{\|\boldsymbol{\beta}_B\|}{2\|\boldsymbol{B}\|}, & \text{otherwise,} \end{cases}$$

with

$$\boldsymbol{\beta}_B = \frac{|R(u_h)|}{\|\boldsymbol{\nabla} u_h\|^2} \boldsymbol{\nabla} u_h \quad \text{and} \quad \boldsymbol{B} = \boldsymbol{\beta}_B \frac{\partial \boldsymbol{\xi}}{\partial \boldsymbol{x}},$$

where V_e is the volume of the element Ω_e, $\Gamma_+ = \{\boldsymbol{x} \in \Omega_e; \boldsymbol{\beta} \cdot \boldsymbol{n} > 0\}$ is the outflow part of Γ, $\boldsymbol{n}$ is the unit outward normal vector to the boundary Γ, $\boldsymbol{x} = (x, y, z) \in \Omega$ and $\boldsymbol{\xi} = (\xi, \eta, \zeta)$ is the vector whose components are the standard variables.

The method is solved by using an iterative procedure defined as: given u^n, we find $u^{n+1} \in S_E$ satisfying

$$A(u^{n+1}, v) + A_{DD}(u_h^n; u^{n+1}, v) = F(v), \quad \forall v \in V_E, \tag{6}$$

where the initial solution is $u^0 = 0$.

To improve convergence, we consider the weighting rule $\tau_{DD}(u_h^{n+1}) = w\widetilde{\tau}_{DD}(u_h^{n+1}) + (1 - w)\tau_{DD}(u_h^n)$, with $w = 0.5$ and $\widetilde{\tau}_{DD}(u_h^{n+1})$ calculated using the expression (4). The Eq. (6) results in the following local system of algebraic equations, associated with each element Ω_e,

$$\begin{bmatrix} A_{hh}^e & A_{bh}^e \\ A_{hb}^e & A_{bb}^e \end{bmatrix} \begin{bmatrix} U_h^e \\ U_b^e \end{bmatrix} = \begin{bmatrix} F_h^e \\ F_b^e \end{bmatrix}, \tag{7}$$

where the local matrices and vectors in Eq. (7) are defined as follow,

$$A_{hh}^e : \int_{\Omega_e} \Big(\big(\kappa + \tau_{DD}(u_h)\big) \boldsymbol{\nabla} u_h \cdot \boldsymbol{\nabla} v_h + (\boldsymbol{\beta} \cdot \boldsymbol{\nabla} u_h) v_h + \sigma u_h v_h \Big) \; d\Omega_e;$$
$$A_{bh}^e : \int_{\Omega_e} \Big((\boldsymbol{\beta} \cdot \boldsymbol{\nabla} u_b) v_h + \sigma u_b v_h \Big) \; d\Omega_e; \qquad F_h^e : \int_{\Omega_e} f v_h \; d\Omega_e;$$

$$A^e_{hb} : \int_{\Omega_e} \Big((\boldsymbol{\beta} \cdot \boldsymbol{\nabla} u_h) v_b + \sigma u_h v_b \Big)\, d\Omega_e; \qquad F^e_b : \int_{\Omega_e} f v_b \, d\Omega_e;$$
$$A^e_{bb} : \int_{\Omega_e} \Big(\big(\kappa + \tau_{DD}(u_h)\big) \boldsymbol{\nabla} u_b \cdot \nabla v_b + \sigma u_b v_b \Big)\, d\Omega_e;$$

and U^e_h and U^e_b are the vectors that store the variables $u_h|_{\Omega_e}$ and u_b, respectively. Performing a static condensation to eliminate the unknowns U^e_b at each element, the system (7) can be written in terms of the macro solution U^e_h, as follows,

$$\Big(A^e_{hh} - A^e_{bh} (A^e_{bb})^{-1} A^e_{hb} \Big) U^e_h = F^e_h - A^e_{bh} (A^e_{bb})^{-1} F^e_b. \tag{8}$$

Assembling all local systems (8), calculated on each element Ω_e, we obtain the global system,

$$[\boldsymbol{A}_h(\boldsymbol{U}^n_h)] \boldsymbol{U}^{n+1}_h = \boldsymbol{F}_h, \tag{9}$$
$$\boldsymbol{U}^0_h = \boldsymbol{0}. \tag{10}$$

We solved the problem (9)–(10) using the nonlinear scheme described in Algorithm 1 that is based on the damping algorithm given in John and Knobloch [14]. The linear systems are solved by the Generalized Minimal Residual (GMRES) method [30].

When calculating an approximate solution, we are concerned with the accuracy of that solution obtained. The error e is defined as the difference between the exact solution and the approximate solution, $e(\boldsymbol{x}) = u_e(\boldsymbol{x}) - u_h(\boldsymbol{x})$. Normally, the a priori error estimate, measured in an appropriate norm $\|\cdot\|_*$, follows the form

$$\|e\|_* \leq C h^p, \tag{11}$$

where h is mesh parameter, C is a constant that depends on the data of the problem and p represents the convergence rate with respect to the norm $\|\cdot\|_*$ [31]. The error estimates are calculated using the $L^2(\Omega)$, $H^1(\Omega)$ and energy norms, which are defined by

$$\|e\|^2_{L^2(\Omega)} = \int_\Omega |e|^2 d\Omega, \qquad \|e\|^2_{H^1(\Omega)} = \|e\|^2_{L^2(\Omega)} + \|\boldsymbol{\nabla} e\|^2_{L^2(\Omega)},$$
$$\|e\|^2_E = \sigma \|e\|^2_{L^2(\Omega)} + \kappa \|\boldsymbol{\nabla} e\|^2_{L^2(\Omega)}.$$

The H^1 and energy norms provide similar measures of the error under certain conditions, but as the H^1 norm does not depend on the problem, it is more convenient in some situations.

Using piece-wise linear basis function, the Galerkin finite element method presents, for $u_e \in H^2(\Omega)$, the following a priori error estimates: $\|e\|_{L^2(\Omega)} \leq C h^2$ and $\|e\|_{H^1(\Omega)} \leq C h$, whereas most linear stabilized methods present $\|e\|_{L^2(\Omega)} \leq C h^{3/2}$ and $\|e\|_{H^1(\Omega)} \leq C h$ [9,11,12,15].

Algorithm 1: Nonlinear algorithm

Data: $u_h^0 := 0$; $r^0 := \|f\|$; $w_{min} := 0.01$; $w_{max} := 1.0$;
$c_1 := 1.001$; $c_2 := 1.1$; $c_3 := 1.001$; $c_4 := 0.9$;
Result: Solution u_h of the system (9)-(10).

$w := w_{max}$; $k := 0$; $er := r^0$;
while $er > Tol$ **and** $k < MaxIter$ **do**
  compute $\tilde{u}_h^{k+1}$ satisfying Eq. (9);
  $firstDamp := 1$; $aux := 1$;
  while $aux = 1$ **do**
    $u_h^{k+1} := u_h^k + w(\tilde{u}_h^{k+1} - u_h^k)$;
    compute residual r^{k+1} using Eq. (5);
    if $r^{k+1} < r^k$ **or** $w \leq c_1 w_{min}$ **then**
      if $r^{k+1} < r^k$ **and** $firstDamp = 1$ **then**
        $w_{max} := min(1, c_3 w_{max})$;
        $w := min(w_{max}, c_2 w)$;
      end
      $aux := 0$;
    else
      $w := max(w_{min}, w/2)$;
      if $firstDamp = 1$ **then**
        $w_{max} := max(w_{min}, c_4 w_{max})$;
        $firstDamp := 0$;
      end
    end
  end
  compute absolute error $er = \|u^{k+1} - u^k\|$;
  $k = k + 1$;
end

In order to evaluate numerically the convergence rate, p, given in (11), we define the function $\mathcal{E}(h) = Ch^p$ and plot the graph of $\log \mathcal{E} = p \log h + \log C$ in terms of $\log h$, resulting in a straight line whose slope is p. Thus, for h sufficiently small, a plot of $\log \|e\|_*$ versus $\log h$ will give a straight line with slope equal to p. The 3D integrals present in the definition of $\|\cdot\|_{L^2(\Omega)}$, $\|\cdot\|_{H^1(\Omega)}$ and $\|\cdot\|_E$ are solved numerically using Gaussian quadrature considering tetrahedral elements whose weights and points are described in [32].

3 Numerical Experiments

In this section, we obtain the convergence rates for a diffusion-convection problem and for a diffusion-convection-reaction problem in a unit cube, considering two set of meshes generated and refined using Gmsh [33]: GRID 1 (structured meshes), generated by dividing for 4, 8, 16, 32, 64 parts in each direction; and

GRID 2 (unstructured meshes), generated by starting with the value of the element size factor at 0.25 in the 8 points that generate the domain and dividing by 2 to obtain a new, more refined mesh. Table 1 shows the number of nodes and elements for all meshes.

Table 1. Size of the meshes using in the experiments.

(a) GRID 1

Meshes	Nodes	Elements
M1	125	384
M2	729	3072
M3	4913	24576
M4	35937	196608
M5	274625	1572864

(b) GRID 2

Meshes	Nodes	Elements
M6	141	373
M7	685	2564
M8	4014	18932
M9	27458	148982
M10	200742	1169024

The mesh Péclet number, $Pe = \frac{\|\boldsymbol{\beta}\|h}{2\kappa}$, expresses the relationship between convective and diffusive effects on a mesh with size h. It indicates if the numerical solution is convection or diffusion-dominated. When $Pe > 1$ or $\kappa < \frac{\|\boldsymbol{\beta}\|h}{2}$ the numerical approximation is convection-dominated or the mesh is too coarse. In this case the Galerkin finite element method may present unphysical solution in problems with boundary and internal layers, requiring a stabilization scheme. When $Pe \leq 1$ the numerical solution is diffusion-dominated and the classical Galerkin finite element methods perform well.

Table 2. Mesh Péclet numbers in the meshes.

Meshes		Mesh Péclet numbers (Pe)		
		$\kappa = 1$	$\kappa = 10^{-3}$	$\kappa = 10^{-6}$
GRID 1	M1	1.19×10^{-1}	1.19×10^{2}	1.19×10^{5}
	M2	5.95×10^{-2}	5.95×10^{1}	5.95×10^{4}
	M3	2.97×10^{-2}	2.97×10^{1}	2.97×10^{4}
	M4	1.48×10^{-2}	1.48×10^{1}	1.48×10^{4}
	M5	7.44×10^{-3}	7.44×10^{0}	7.44×10^{3}
GRID 2	M6	1.67×10^{-1}	1.67×10^{2}	1.67×10^{5}
	M7	8.44×10^{-2}	8.44×10^{1}	8.44×10^{4}
	M8	4.64×10^{-2}	4.64×10^{1}	4.64×10^{4}
	M9	2.25×10^{-2}	2.25×10^{1}	2.25×10^{4}
	M10	1.10×10^{-2}	1.10×10^{1}	1.10×10^{4}

This error estimates study considers different values of Pe. The mesh size is defined as $h = \sqrt[3]{V}$, where $V = \max\{V_e\}$ is the volume of the largest element

of the mesh. In both problems, $\boldsymbol{\beta} = (1, 1, 1)^T$. Therefore, the problems studied here vary the value of κ having a problem of dominant diffusion when $\kappa = 1$ and dominant convection when $\kappa = 10^{-3}$ and $\kappa = 10^{-6}$. Table 2 shows the Pe for the thickest and most refined mesh of each set of mesh types. As one can see, for dominant diffusion problem ($\kappa = 1$), $Pe < 1$ and for dominant convection problems ($\kappa = 10^{-3}$ and $\kappa = 10^{-6}$), $Pe > 1$ and the value of Pe increases when κ decreases.

Figure 1 presents the structured mesh M3 and the unstructured mesh M8. In Fig. 1a (structured mesh) the elements have the same size and are distributed in an organized way, whereas in Fig. 1b (unstructured mesh) the elements have similar sizes but are not organized.

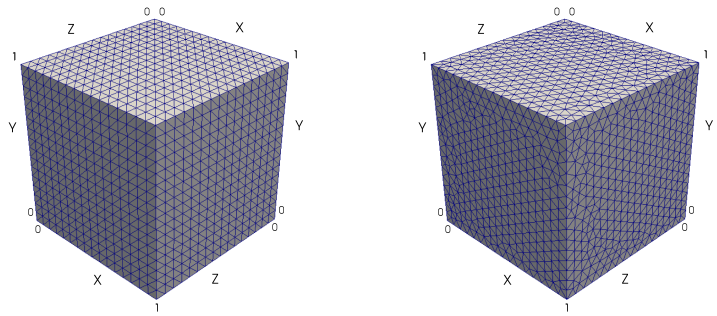

(a) M3 (GRID 1) **(b)** M8 (GRID 2)

Fig. 1. Visualization of the two types of meshes used.

The computational code was developed in C language in a computer with the following characteristics: Intel Corel $i5 - 2450M$, CPU 2.50 GHz $\times 4$ and 8 GB of RAM. The linear systems are solved with the GMRES method considering 50 Krylov vectors to restart, ILU(1) preconditioner, the maximum number of 100 cycles and a tolerance of 10^{-7}. For the nonlinear algorithm we use a tolerance of 10^{-3} and maximum number of iterations of 300. Due to the difficulty of visualizing solutions in three-dimensional domains, we present the solutions on the line passing through the cube diagonal, that is, a line that passes through points $(0, 0, 0)$ and $(1, 1, 1)$.

3.1 Diffusion-Convection (DC) Problem

Consider a DC problem in the unit cube $\Omega =]0, 1[^3$ with a smooth exact solution given by $u(x, y, z) = sin(\pi x)sin(\pi y)sin(\pi z)$ and coefficients, $\boldsymbol{\beta} = (1, 1, 1)^T$, $\sigma = 0$, $\kappa \in \{1, 10^{-3}, 10^{-6}\}$, so that the source term and the Dirichlet boundary conditions satisfy the exact solution.

Figures 2 and 3 show the solutions obtained by the DD method on all meshes, for each $\kappa \in \{1, 10^{-3}, 10^{-6}\}$. In terms of convergence, the results obtained for the GRID 1, Fig. 2, and for the GRID 2, Fig. 3, are similar. Although the DD solutions on the coarsest meshes (M1 for GRID 1 and M6, M7 for GRID 2) are not quite accurate, when the meshes are refined, the solutions approach the exact solution, for all values of κ.

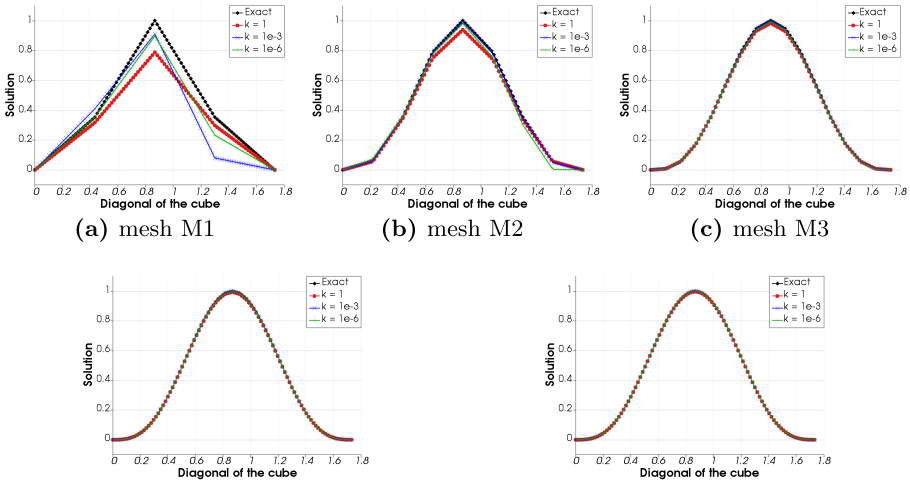

(a) mesh M1 **(b)** mesh M2 **(c)** mesh M3

(d) mesh M4 **(e)** mesh M5

Fig. 2. Solution of DC problem at the cube diagonal – $\kappa = 1,\ 10^{-3},\ 10^{-6}$ – GRID 1

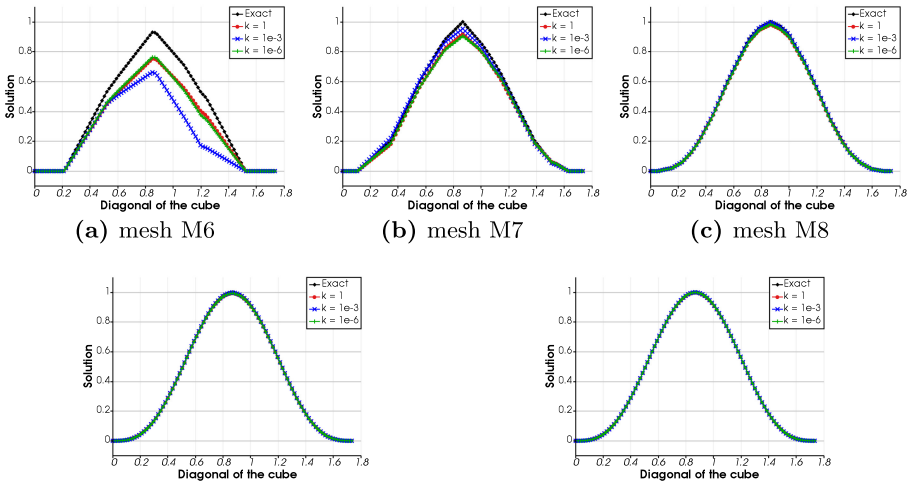

(a) mesh M6 **(b)** mesh M7 **(c)** mesh M8

(d) mesh M9 **(e)** mesh M10

Fig. 3. Solution of DC problem at the cube diagonal – $\kappa = 1,\ 10^{-3},\ 10^{-6}$ – GRID 2.

Figures 4, 5 and 6 present the convergence rates in the $L^2(\Omega)$, $H^1(\Omega)$ and energy norms for GRID 1 and 2 considering $\kappa = 1,\ 10^{-3}$ and 10^{-6}, respectively. In the convection-dominated case, shown in Fig. 5 ($\kappa = 10^{-3}$) and Fig. 6 ($\kappa = 10^{-6}$), optimal convergence rates are obtained for all set of meshes in both norms, $L^2(\Omega)$ and $H^1(\Omega)$. In the diffusion dominated case, Fig. 4 ($\kappa = 1$), also optimal convergence rates are obtained in the $H^1(\Omega)$ norm for both grids, whereas the $L^2(\Omega)$ norm presents a rate higher than the suboptimal one.

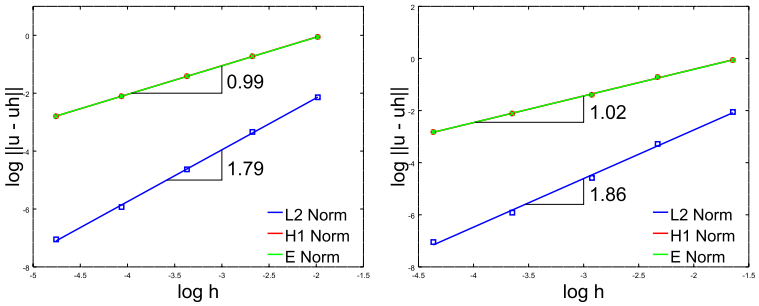

(a) GRID 1 **(b)** GRID 2

Fig. 4. Convergence rates considering the DC problem with $\kappa = 1$.

For the DC problem, $\sigma = 0$ and the energy norm satisfies $\|e\|_E = \sqrt{\kappa}\|\boldsymbol{\nabla} e\|_{L^2(\Omega)} = \sqrt{\kappa}|e|_{H^1(\Omega)}$, where $|\cdot|_{H^1(\Omega)}$ is the usual semi-norm of the space $H^1(\Omega)$ and which presents the same convergence rate of the $H^1(\Omega)$ norm, for solutions $u \in H_0^1(\Omega)$, as shown in Figs. 5, 6 and 4.

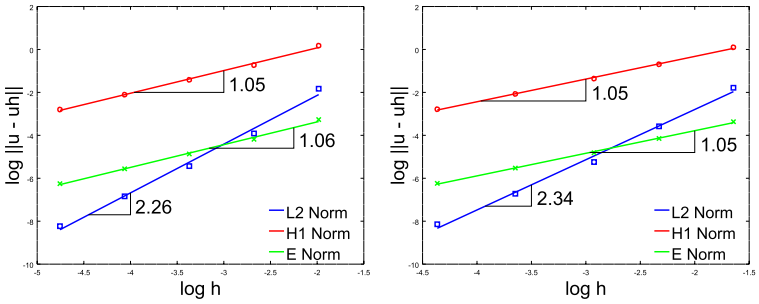

(a) GRID 1 **(b)** GRID 2

Fig. 5. Convergence rates considering the DC problem with $\kappa = 10^{-3}$.

When $\kappa = 1$, Fig. 4, the error in the $H^1(\Omega)$ norm is slightly greater than the error in energy norm, so that graphically, the two lines are superimposed

and look like a single line. As κ decreases, the energy norm error also decreases, which causes its convergence rate line to move away from the $H^1(\Omega)$ norm rate line, but with the same slope (convergence rate), according to Figs. 5 and 6.

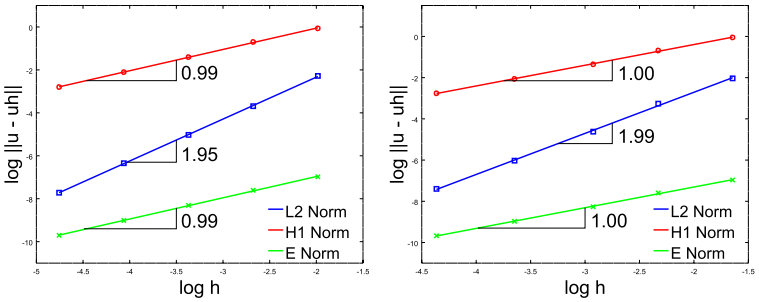

(a) GRID 1 **(b)** GRID 2

Fig. 6. Convergence rates considering the DC problem with $\kappa = 10^{-6}$.

3.2 Diffusion-Convection-Reaction (DCR) Problem

In this experiment, we consider a DCR problem, defined in $\Omega =]0, 1[^3$, with a smooth exact solution, $u(x, y, z) = 100xyz(1-x)(1-y)(1-z)$ and coefficients, $\boldsymbol{\beta} = (1, 1, 1)^T$, $\sigma = 1$, $\kappa \in \{1, 10^{-3}, 10^{-6}\}$, so that the source term and the Dirichlet boundary conditions satisfy the exact solution.

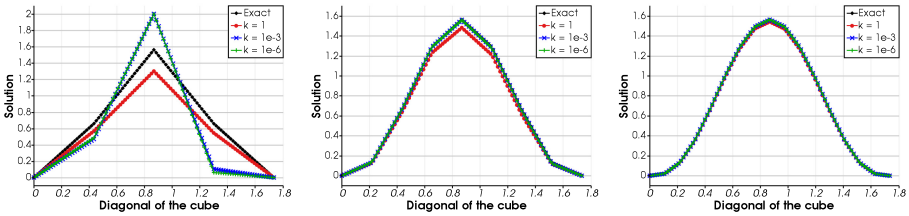

(a) mesh M1 **(b)** mesh M2 **(c)** mesh M3

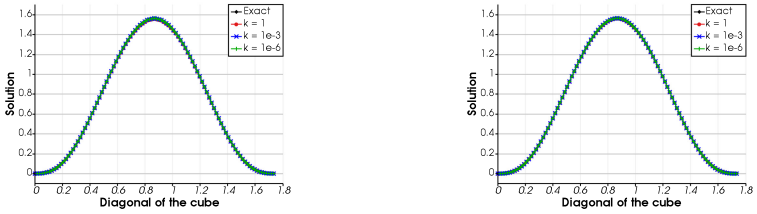

(d) mesh M4 **(e)** mesh M5

Fig. 7. Solution of DCR problem at the cube diagonal – $\kappa = 1,\ 10^{-3},\ 10^{-6}$ – GRID 1.

Figures 7 and 8 present the DD solutions and the exact solution to the DCR problem considering $\kappa = 1,\ 10^{-3},\ 10^{-6}$, respectively, for both set of meshes. As one can see for GRID 1 and GRID 2 the behavior of the DD solutions for DCR problem are very similar with those obtained for DC problem. In general, the DD solutions are closer to the exact solution when the mesh is refined.

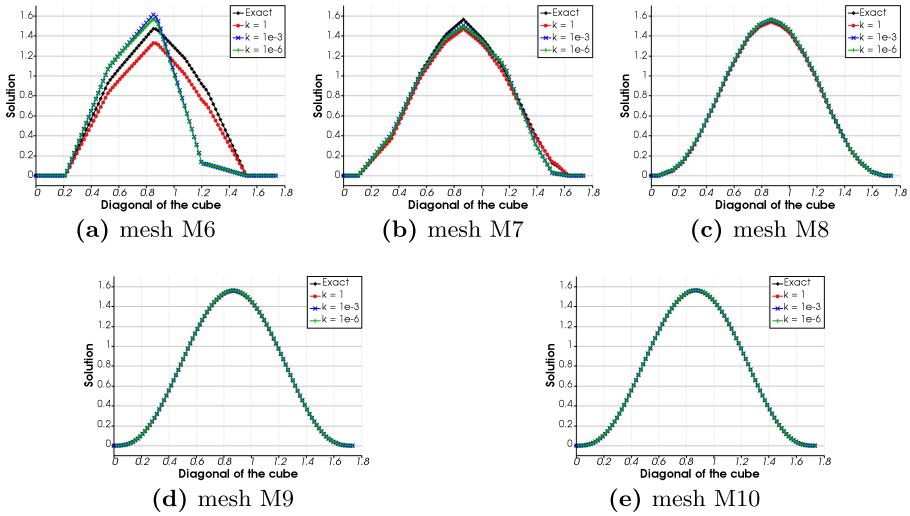

(a) mesh M6 **(b)** mesh M7 **(c)** mesh M8

(d) mesh M9 **(e)** mesh M10

Fig. 8. Solution of DCR problem at the cube diagonal – $\kappa = 1,\ 10^{-3},\ 10^{-6}$ – GRID 2.

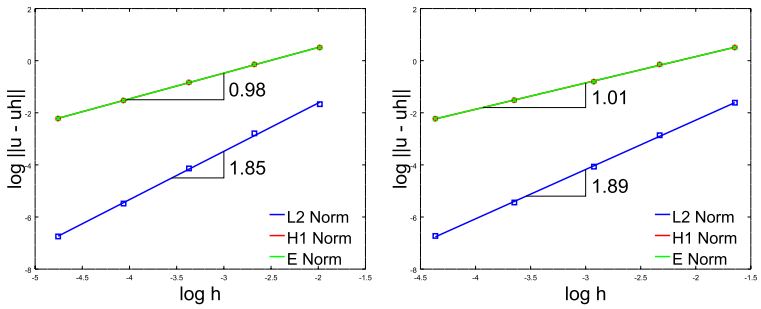

(a) GRID 1 **(b)** GRID 2

Fig. 9. Convergence rates considering the DCR problem with $\kappa = 1$.

Figures 9, 10 and 11 present the convergence rates in the $L^2(\Omega)$, $H^1(\Omega)$ and energy norms for GRID 1 and 2, respectively, considering $\kappa = 1,\ 10^{-3},\ 10^{-6}$ for the three dimensional DCR problem. The convergence rates present a behavior similar to the case of the CD problem: convection dominant problems obtained optimal rates for all set of meshes, whereas for diffusion dominated case, the $L^2(\Omega)$ norm presents a rate higher than the suboptimal one for both grids.

When $\kappa = 1$ the energy norm is precisely the $H^1(\Omega)$ norm, which can be seen in Fig. 9. When $\kappa = 10^{-6}$, the zero-order term outweighs the first-order term so that the energy norm is close to the $L^2(\Omega)$ norm, as shown in Fig. 11. When $\kappa = 10^{-3}$, the contribution of the term containing the gradient of the error affects the convergence rate. Thus, the rate presented by the energy norm is of order $\mathcal{O}(h^{1.5})$.

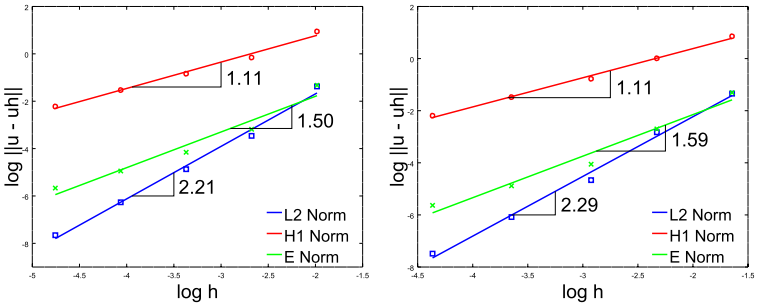

(a) GRID 1 **(b)** GRID 2

Fig. 10. Convergence rates considering the DCR problem with $\kappa = 10^{-3}$.

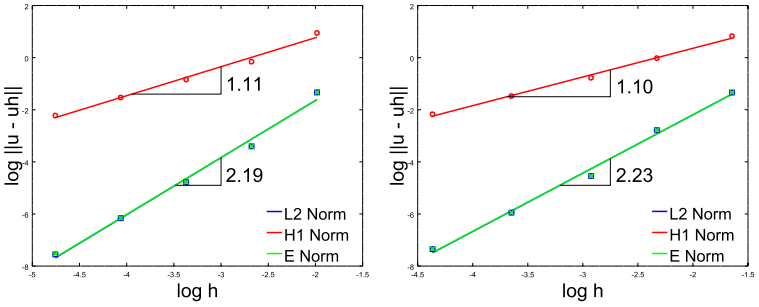

(a) GRID 1 **(b)** GRID 2

Fig. 11. Convergence rates considering the DCR problem with $\kappa = 10^{-6}$.

4 Conclusions

This work presents a convergence rate evaluation of the DD method applied to the three-dimensional stationary transport equation, considering diffusion-convection and diffusion-convection-reaction problems. Experiments were carried out when diffusion was dominant, $\kappa = 1$, and when convection was dominant, $\kappa = 10^{-3}$ and $\kappa = 10^{-6}$, considering two set of meshes: one structured and another unstructured.

In both problems we observed that when the convection is dominant, the method presented an optimal convergence in $L^2(\Omega)$ norm, i.e., $\mathcal{O}(h^2)$ and in $H^1(\Omega)$ norm, i.e., $\mathcal{O}(h^1)$. However, when the diffusion is dominant, the method presented a rate higher than the suboptimal one in $L^2(\Omega)$ norm, i.e., approximately $\mathcal{O}(h^{1.8})$ and an optimal convergence in $H^1(\Omega)$ norm, i.e., $\mathcal{O}(h^1)$.

The energy norm presented the behavior that was expected. In the DC problem, it presented a convergence rate equal to the rate of the $H^1(\Omega)$ norm, $\mathcal{O}(h^1)$, whereas for the DCR problem, the convergence rate varies according to the κ variation, agreeing with the $H^1(\Omega)$ and $L^2(\Omega)$ result for $\kappa = 1$ and $\kappa = 10^{-6}$. When $\kappa = 10^{-3}$, it presented a convergence rate in the order $\mathcal{O}(h^{1.5})$.

As a future work, we will apply this methodology to solve three-dimensional transient transport problems and also to investigate the convergence rates in suitable norms.

Acknowledgments. This work was supported by the Espírito Santo State Research Support Foundation (FAPES), under Grant Term 181/2017, and by the Coordenação de Aperfeiçoamento de Pessoal de Nível Superior - Brasil (CAPES) - Finance Code 001.

References

1. Friedman, A., Littman, W.: Industrial mathematics: a course in solving real-world problems. Society for Industrial and Applied Mathematics, pp. 27–45 (1994)
2. Kuttler, C.: Reaction-Diffusion equations with applications. In: Internet siminar, Technische Unversität München, pp. 3–11 (2011)
3. Jüngel, A.: Diffusive and nondiffusive population models. In: Naldi, G., Pareschi, L., Toscani, G. (eds) Mathematical Modeling of Collective Behavior in Socio-Economic and Life Sciences. Modeling and Simulation in Science, Engineering and Technology, pp 397–425. Birkhäuser Boston (2010) https://doi.org/10.1007/978-0-8176-4946-3_15
4. Colombo, R.M., Garavello, M., Lécureux-Mercier, M.: A class of nonlocal models for pedestrian traffic. Math. Models Methods Appl. Sci. **22**(04), 1150023 (2012). https://doi.org/10.1142/S0218202511500230
5. Lopes, R.J.G., Quinta-Ferreira, R.M.: Numerical assessment of diffusion-convection-reaction model for the catalytic abatement of phenolic wastewaters in packed-bed reactors under trickling flow conditions. Comput. Chem. Eng. **35**(12), 2706–2715 (2011)
6. Yin, S., Towler, B.F., Dusseault, M.B., Rothenburg, L.: Fully coupled THMC modeling of wellbore stability with thermal and solute convection considered. Transp. Porous Media **84**(3), 773–798 (2010). https://doi.org/10.1007/s11242-010-9540-9
7. Quarteroni, A.: Numerical Models for Differential Problems, vol. 16. Springer, Cham (2017). https://doi.org/10.1007/978-3-319-49316-9_21
8. Brooks, A.N., Hughes, T.J.R.: Streamline upwind Petrov-Galerkin formulations for convection dominated flows with particular emphasis on the incompressible Navier-Stokes equations. Comput. Methods Appl. Mech. Eng. **32**(1–3), 199–259 (1982)

9. Hughes, T.J.R., Franca, L.P., Hulbert, G.M.: A new finite element formulation for computational fluid dynamics: VIII. The Galerkin/Least-Squares method for advective-diffusive equations. Comput. Methods Appl. Mech. Eng. **73**(2), 173–189 (1989)
10. Franca, L., Valentin, F.: On an improved unusual stabilized finite element method for the advective-reactive-diffusive equation. Comput. Methods Appl. Mech. Eng. **190**(13), 1785–1800 (2000). https://doi.org/10.1016/S0045-7825(00)00190-0
11. Burman, E., Hansbo, P.: Edge stabilization for Galerkin approximations of convection-diffusion-reaction problems. Comput. Methods Appl. Mech. Eng. **193**(15), 1437–1453 (2004)
12. Knobloch, P., Lube, G.: Local projection stabilization for advection-diffusion-reaction problems: one-level vs. two-level approach. Appl. Numer. Math. **59**(12), 2891–2907 (2009)
13. John, V., Knobloch, P.: On spurious oscillations at layers diminishing (SOLD) methods for convection-diffusion equations: part I-a review. Comput. Methods Appl. Mech. Eng. **196**(17), 2197–2215 (2007)
14. John, V., Knobloch, P.: On spurious oscillations at layers diminishing (SOLD) methods for convection-diffusion equations: part II - analysis for P1 and Q1 finite elements. Comput. Methods Appl. Mech. Eng. **197**(21–24), 1997–2014 (2008)
15. Johnson, C., Nävert, U., Pitkäranta, J.: Finite element methods for linear hyperbolic problems. Comput. Methods Appl. Mech. Eng. **45**(1), 285–312 (1984). https://doi.org/10.1016/0045-7825(84)90158-0
16. Allendes, A., Barrenechea, G., Rankin, R.: Fully computable error estimation of a nonlinear, positivity-preserving discretization of the convection-diffusion-reaction equation. SIAM J. Sci. Comput. **39**(5), A1903–A1927 (2017). https://doi.org/10.1137/16M1092763
17. Barrenechea, G.R., John, V., Knobloch, P.: A local projection stabilization finite element method with nonlinear crosswind diffusion for convection-diffusion-reaction equations. ESAIM Math. Model. Numer. Anal. **47**(5), 1335–1366 (2013)
18. Barrenechea, G.R., Burman, E., Karakatsani, F.: Blending low-order stabilised finite element methods: A positivity-preserving local projection method for the convection-diffusion equation. Comput. Methods Appl. Mech. Eng. **317**, 1169–1193 (2017)
19. Hughes, T.J.R.: Multiscale phenomena: green's functions, the Dirichlet-to-Neumann formulation, subgrid scale models, bubbles and the origins of stabilized methods. Comput. Methods Appl. Mech. Eng. **127**(1–4), 387–401 (1995)
20. Hughes, T.J., Feijóo, G.R., Mazzei, L., Quincy, J.B.: The variational multiscale method - a paradigm for computational mechanics. Comput. Methods Appl. Mech. Eng. **166**(1–2), 3–24 (1998)
21. Arruda, N.C.B., Almeida, R.C., Dutra do Carmo, E.G.: Dynamic diffusion formulations for advection dominated transport problems. In: Dvorkin, E., Goldschmit, M., Storti, M. (eds.) Mecánica Computacional, vol. 29, pp. 2011–2025. Asociación Argentina de Mecánica Computacional, Buenos Aires (2010)
22. Baptista, R., Bento, S.S., Santos, I.P., Lima, L.M., Valli, A.M.P., Catabriga, L.: A multiscale finite element formulation for the incompressible Navier-Stokes equations. In: Gervasi, O., et al. (eds.) ICCSA 2018. LNCS, vol. 10961, pp. 253–267. Springer, Cham (2018). https://doi.org/10.1007/978-3-319-95165-2_18
23. Bento, S.S., de Lima, L.M., Sedano, R.Z., Catabriga, L., Santos, I.P.: A nonlinear multiscale viscosity method to solve compressible flow problems. In: Gervasi, O., et al. (eds.) ICCSA 2016. LNCS, vol. 9786, pp. 3–17. Springer, Cham (2016). https://doi.org/10.1007/978-3-319-42085-1_1

24. Santos, I.P., Almeida, R.C.: A nonlinear subgrid method for advection-diffusion problems. Comput. Methods Appl. Mech. Eng. **196**(45–48), 4771–4778 (2007)
25. Santos, I., Almeida, R., Malta, S.: Numerical analysis of the nonlinear subgrid scale method. Comput. Appl. Math. **31**(3), 473–503 (2012)
26. Valli, A.M.P., Almeida, R.C., Santos, I.P., Catabriga, L., Malta, S.M.C., Coutinho, A.L.G.A.: A parameter-free dynamic diffusion method for advection-diffusion-reaction problems. Comput. Math. Appl. **75**(1), 307–321 (2018)
27. Azevedo, R.Z.S., Santos, I.P.: Multiscale finite element formulation for the 3D diffusion-convection equation. In: Gervasi, O., et al. (eds.) ICCSA 2020. LNCS, vol. 12251, pp. 455–469. Springer, Cham (2020). https://doi.org/10.1007/978-3-030-58808-3_33
28. Santos, I.P., Malta, S.M., Valli, A.M., Catabriga, L., Almeida, R.C.: Convergence analysis of a new dynamic diffusion method (2021, submitted)
29. Ern, A., Guermond, J.-L.: Theory and Practice of Finite Elements. vol. 159. 1st edn. Springer, New York (2004). https://doi.org/10.1007/978-1-4757-4355-5
30. Saad, Y., Schultz, H.: GMRES: a generalized minimal residual algorithm for solving nonsymmetric linear systems. SIAM. J. Sci. Stat. Comput. **7**(3), 856–869 (1986)
31. Becker, E.B., Carey, G.F., Oden, J.T.: Finite Elements - An Introduction, vol. 1. Prentice-Hall, New Jersey (1981)
32. Zienkiewicz, O.C., Taylor, R.L.: The Finite Element Method - Volume 1: The Basis, 5th edn. Butterworth-Heinemann, Massachusetts (2000)
33. Geuzaine, C., Remacle, J.F.: Gmsh: a three-dimensional finite element mesh generator with built-in pre- and post-processing facilities. Int. J. Num. Methods Eng. **79**(11), 1309–1331 (2009). https://gmsh.info